High Detectivity Perovskites Light Detectors Printed in Air from Benign Solvents

Vijay Venugopalan[±1], Roberto Sorrentino[±1,2], Peter Topolovsek[±1,3], Diego Nava[1,2], Stefanie Neutzner[1], Giorgio Ferrari[3], Annamaria Petrozza[1*], Mario Caironi[1*]

[1]Center for Nano Science and Technology @PoliMi, Istituto Italiano di Tecnologia, via G. Pascoli 70/3, 20133, Milan, Italy

[2]Dipartimento di Fisica, Politecnico di Milano, Piazza L. da Vinci 32, Milano 20133, Ital

[3]Jožef Stefan International Postgraduate School, Jamova 39, 1000 Ljubljana, Slovenia

[4]Dipartimento di Elettronica, Informazione e Bioingegneria, Politecnico di Milano, Piazza L. da Vinci 32, 20133, Milano, Italy

[±] *Equally contributing authors*

* *Corresponding authors:* mario.caironi@iit.it; annamaria.petrozza@iit.it.

Efficient light detection by solution processed devices can impact a broad range of scientific and technological applications, from security to communication, automation and healthcare. The excellent photoconversion properties of hybrid perovskites semiconductors have been exploited in this direction, but harsh processing solvents and highly controlled growth conditions limit their applicability. Here we propose a simple and low temperature approach for the synthesis of methylammonium lead halide perovskite inks based on sub-micrometer sized particles with tunable band-gap. The particles allow to formulate inks in benign solvents, such as isopropanol, and to print

under ambient conditions the photoactive layers of planar photoconductors with scalable, large-area coating techniques. When surface traps are passivated with [6,6]-phenyl-C61-butyric acid methyl ester fullerene (PCBM), a high photoconductive gain, exceeding 200 in the blue, and reduced noise, produce record high Specific Detectivities exceeding 7 × 10^{13} cmHz$^{0.5}$/W, and Gain-Bandwidth product values of 7.5 × 10^{6} Hz. Given the extreme simplicity of the presented device architecture and the straightforward processing, yielding printable light detectors rivalling established technologies, the present work promises a short time deployment of printed perovskite detectors in a multitude of opto-electronic applications.

Halide perovskite semiconductors have the potential to merge the highly efficient operational principles of conventional inorganic semiconductors with the low-temperature solution processability of emerging organic and hybrid materials. Since the first two reports on high efficiency, solution processed, solid-state hybrid perovskite based solar cells in 2012,[1, 2] there has been a world-wide explosion of activities on these materials, with laboratory scale solar cells power conversion efficiencies recently exceeding 22%.[3] The growing interest in 3D hybrid perovskite semiconductors has soon expanded their field of application, with proof of concept electroluminescent and lasing devices,[4] thus potentially impacting optoelectronics under many aspects. Light detection is one of the fields where there is large potential for achieving real applications in a short to medium time-frame. In fact light detectors require some of the key properties that make halide perovskite a good material for solar cells, while moving the competition with existing technologies from a difficult "cost per Watt peak" scenario to a cost per functionality one. Notably, large absorption coefficients of 10^{5} cm^{-1} in the visible and UV range, and long carrier lifetimes allow to closely match, or even to exceed, Si photodiodes performances.[5, 6, 7, 8, 9, 10] On top, solution processability would result in a drastic simplification

and affordability of the manufacturing processes, leaving ample room for advanced pixel and array design for imaging applications, for example. Nevertheless, there are a few aspects that currently limit the potential of perovskites for light detection and in general their use for consumer electronics. The toxicity of lead-based compounds is probably the most discussed topic, thus intense research is already tackling the development of lead-free materials. Moreover recent studies are also raising the argument of the possibility of full re-cycling the lead present in exhaust car batteries[11] or in active layer of the opto-electronic devices,[12] thus getting away from the practical and expensive issue of disposal of hazardous materials. Another important aspect regards the organic solvents most often used to prepare perovskite precursor solutions, which present health and environmental hazards.[13] Furthermore, typical solvents employed in the processing of lead halide-based perovskites possess high boiling points. These aspects complicate the deployment of energy efficient fabrication processes and increases the environmental impact and the cost of waste handling. On top of that, the precursors-based approach restricts the available process window.[14, 15, 16, 17, 18] In fact the final microstructure, which dominates the optoelectronics properties of the light absorbing layers, depends on how the constituent ions self-assemble during crystallization on the selected substrate, a complex function of precursor ratio, solvents, processing additives, substrate roughness and surface energy, atmospheric/environmental conditions, annealing temperature and treatment time.

Both the use of hazardous solvents and the difficult control of the polycrystalline structure may limit the potential advantages presented by this emerging technology. Particle-based ink formulations in safer and more environmentally friendly solvents can represent a successful strategy to fully deploy the technology. Various synthetic procedures for fully inorganic[19] or hybrid organic/inorganic[20, 21] lead halide-based perovskite particles have been reported. Among these procedures, colloidal synthesis has the advantage of allowing a high control and tailoring of the morphological and optoelectronic properties of the semiconductor crystals before

deposition, thus helping in the standardization and reproducibility of the subsequently produced films. However, so far, the nanocrystals suspensions are predominantly stabilized by the use of long ligands that are, together with the remnants of high boiling point solvents, difficult to remove. Their complete removal thus requires annealing at elevated temperatures that already overlap with the temperature range where some sensitive perovskite compounds start to deteriorate. This, of course, hampers the fabrication of thin films of good optoelectronic quality. Recently, successful approaches involving the use of shorter ligands have been tested,[19] though a full tunability of the spectral range is not yet achievable due to a lack of stability of colloidal suspensions. Moreover, owing to the low concentration of the inks used to hinder aggregation, achieving the required thickness of the semiconductor layer often requires multiple deposition steps. Alternative syntheses of methylammonium lead halide perovskite nanoparticles were also proposed, based on laser ablation,[22] grinding of the solid perovskite components,[23] ultrasonication of components[24, 25, 26] or a combination of grinding and sonication.[27] However, all these methodologies still utilize growth controlling capping ligands and/or are hardly scalable and/or involve the use of expensive, high boiling point and often hazardous solvents.

Here we report a straightforward and scalable low temperature synthesis of methylammonium lead tri-iodide ($MAPbI_3$) perovskite particles with tunable dimensions, down to the submicrometer range, based on a cyclic size reduction process of PbI_2, a solid precursor for perovskite particle synthesis. In contrast to previously reported synthetic procedures, our approach employs only water and isopropanol (IPA), which are widely utilized across industrial, medical and household applications and present much lower health hazard and environmental toxicity concerns in comparison to other commonly used solvents.[13, 28] Synthesized particles are formulated into printable inks with IPA, without additives. Subsequently they are deposited by a large-area bar coating technique[29], and coated with a thin

[6,6]-phenyl-C61-butyric acid methyl ester fullerene (PCBM) layer, which passivates surface traps, accepts electrons and ensures selective charge circulation of holes. This strategy permits to demonstrate the highest measured specific detectivity in printed light detectors till date, [14, 15, 16, 17, 18, 30, 31, 32, 33] reaching a maximum value of 7.23 x 10^{13} cm $Hz^{0.5}$/W in the visible spectrum, even higher than in commercially available Si photodiodes. Moreover, the gain and response time are at least one order of magnitude higher and lower, respectively, than in any other printed perovskite photodetector, allowing to achieve a Gain-Bandwidth product of 7.5 x 10^6 Hz, thereby demonstrating a good balance between signal amplification and device response speed.[34]

Methylammonium lead halide particles synthesis and inks formulation

For the synthesis of $MAPbI_3$ perovskite particles we devised a cyclic approach based on the successive reduction of the size of precursor PbI_2 particles. A schematic illustration of the process is shown in Fig. 1. In the first cycle, the starting PbI_2 precursor is obtained by grinding as-bought PbI_2 powder in a ceramic mortar, under nitrogen atmosphere, to increase its surface area. 200 mg of PbI_2 is slowly added into 10 ml of highly concentrated (100 g/l) methyl ammonium iodide (MAI) solution in isopropanol under stirring at 80 °C. Upon PbI_2 addition into the MAI solution, immediate insertion of MA^+ and I^- ions into the PbI_2 lattice follows, inducing the growth of $MAPbI_3$ cubic-like crystals and turning the MAI solution into a sedimenting dispersion of black perovskite particles. Such formed particles are subsequently isolated through sedimentation and decantation of the residual MAI solution and washed with isopropanol for two times. After this first cycle, we obtain $MAPbI_3$ cubic-like particles with characteristic size of a few (1 to 5) micrometers (see SEM image in Fig. 2a).

The successive cycles allow to reduce the average size of $MAPbI_3$ particles. To start the iteration, the latter are re-dissolved in water, in ambient atmosphere without specific

environmental control. The addition of water promotes rapid extraction of MA^+ and I^- ions from the perovskite lattice that immediately collapses back into water poorly soluble, PbI_2 particles, which were afterwards additionally rinsed with IPA to remove residual MA^+ and I^- ions. The recrystallized PbI_2 particles appear in the form of thin sheets, indicating layered structure of PbI_2, [35] and are smaller in size than the starting PbI_2 precursor. For example, after the first rinse of perovskite particles with water, we obtained PbI_2 sheets with lateral sizes of a few micrometers (Fig. 2b) and thickness of several hundreds of nanometers.

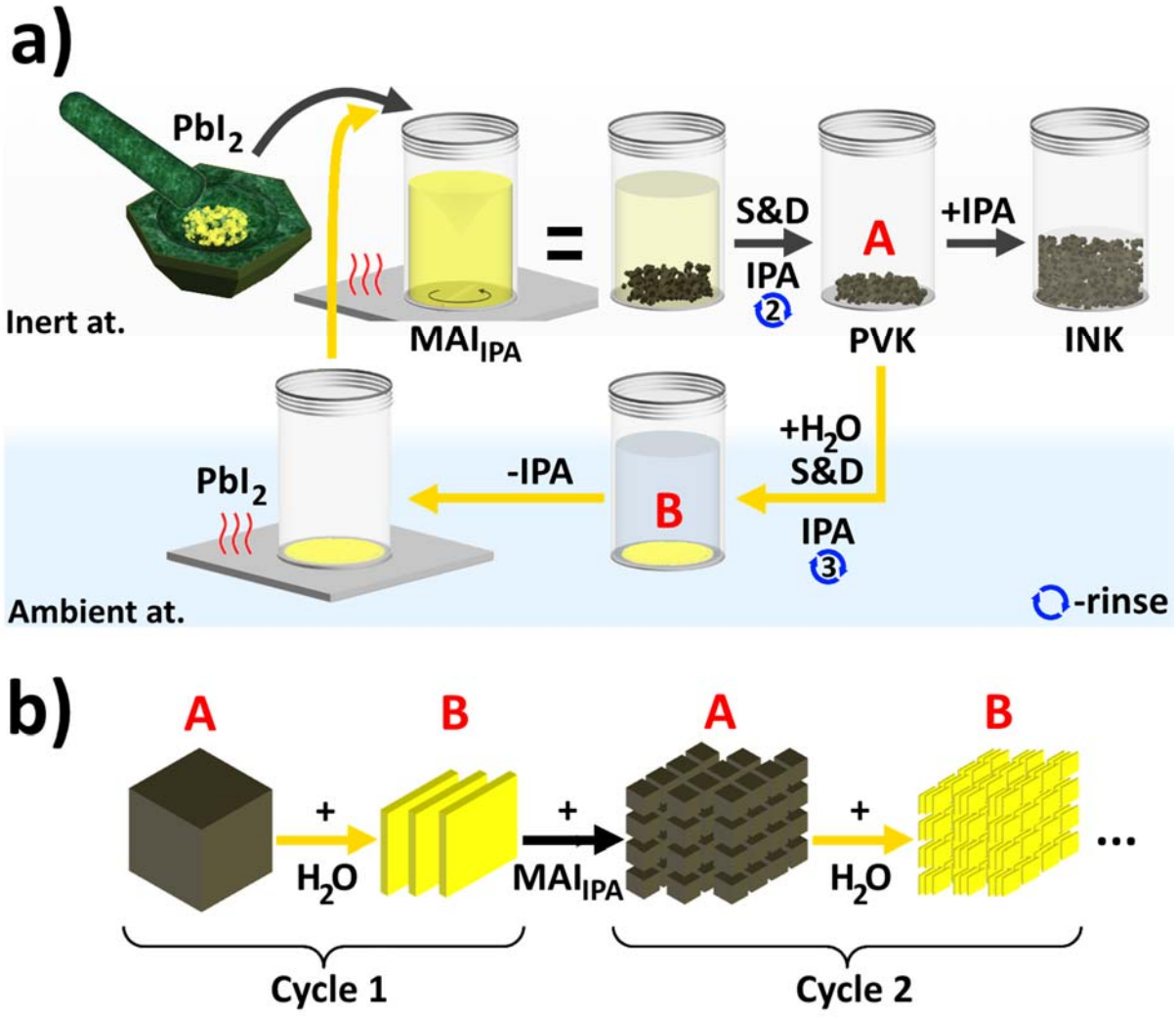

Fig. 1| Synthesis of $MAPbI_3$ particles. a) Schematic representation of cyclic $MAPbI_3$ synthesis, based on three main steps: *i*) addition of PbI_2 (ground, as-bought powder in the first cycle, extracted PbI_2 sheets with smaller dimensions in the following cycles) into a hot MAI

solution under stirring; *ii*) isolation of perovskite particles through sedimentation and decantation (S&D) followed by rinsing with IPA for two times; *iii*) dissolution of perovskite particles in water and precipitation of thin PbI_2 sheets which are isolated through sedimentation and decantation of water solution followed by rinsing with IPA for three times. Such extracted PbI_2 sheets are used as starting precursors for the following steps. b) Scheme of the effect of synthesis cycles on the characteristic size of perovskite particles (A) and lead iodide sheets (B).

The obtained PbI_2 sheets are then adopted as precursors for a new cycle, following the exact same procedure described before, and obtaining sheets with decreasing lateral dimensions and thickness at each step. Starting from smaller PbI_2 sheets, correspondingly smaller cubic perovskites particles can be isolated. Previously, Ha et al. determined a linear relation between the thickness of PbI_2 sheets grown in the [001] direction and the resulting perovskite platelet thickness grown out of it when gas-induced transformation is applied.[36] Assuming that there is no appreciable dissolution neither of PbI_2 or perovskite phase into the MAI solution within the short time frame of particle sedimentation (few minutes), in analogy with the gas-induced transformation where no recrystallization occurs, we infer that the characteristic size of cubic perovskite particles is primarily determined by the PbI_2 sheet thickness.

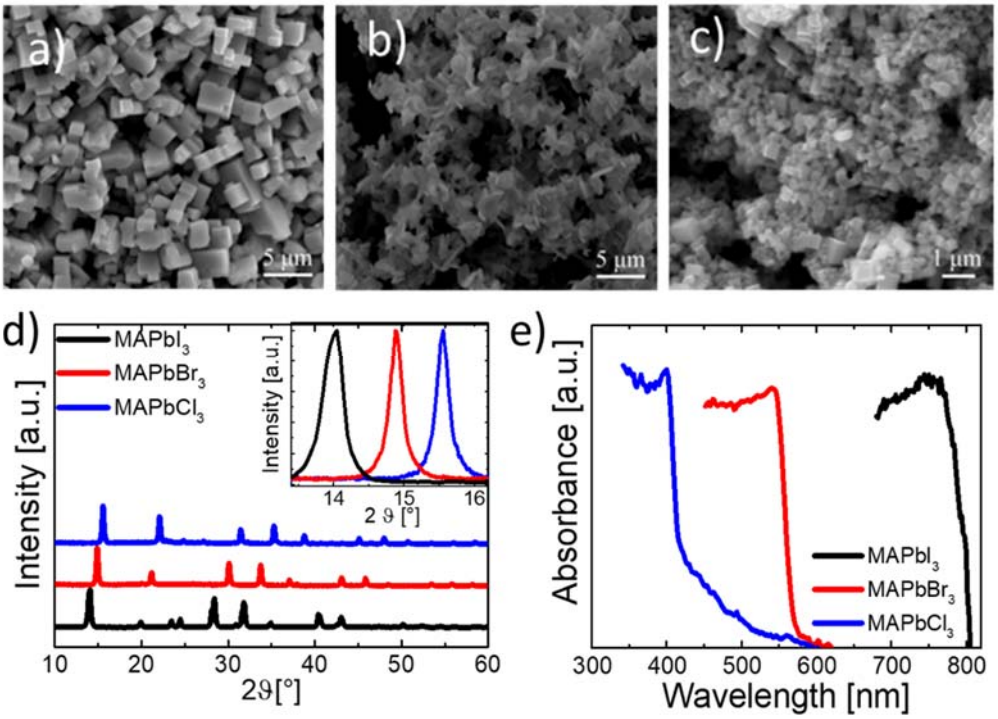

Fig. 2| Characterization of Synthesized Particles. Top view SEM images of (**a**) first cycle synthesis $MAPbI_3$ particles, (**b**) recrystallized PbI_2 sheets and (**c**) final $MAPbI_3$ particles. (**d**) X-Ray diffraction spectra and (**e**) absorption band edges of synthesized $MAPbI_3$, $MAPbBr_3$ and $MAPbCl_3$ particles.

By applying the synthetic cycle three times, we were able to obtain $MAPbI_3$ particles with characteristic size well below 1 µm (Fig. 2c). Such particles are than dispersed in IPA at a concentration of 100mg/ml to obtain a printable ink formulation. Further synthetic cycles do not lead to further reduced particles size. X-ray diffraction measurements show formation of a pure phase of PbI_2 and $MAPbI_3$ at each intermediate step (Fig. S1, in the Supplementary Information, SI) and confirmed that the incorporation of MA^+ and I^- ions into PbI_2 to form $MAPbI_3$ is complete after the final step: the corresponding spectrum (Fig. 2d) shows the characteristic peaks for $MAPbI_3$ at 14.1°, 28.4° and 31.8°, corresponding to the reflection of

the (110), (220) and (310) crystal planes, respectively. No unreacted MAI or PbI_2 (main peaks at 10° and 12.7°, respectively) were detected.

Starting from the synthesized $MAPbI_3$ particles, tuning of the energy bandgap can be achieved through halide exchange. Halide exchange in the $MAPbX_3$ lattice has been previously reported and it is a facile strategy to tune the semiconductor bandgap. Starting from $MAPbI_3$, $MAPbBr_3$ or $MAPbCl_3$, full conversion or mixed halide perovskite ($MAPbI_{3-x}Br_x$, $MAPbI_{3-x}Cl_x$, $MAPbBr_{3-x}Cl_x$), can be obtained depending on the stirring time. This reaction occurs if the solution containing $MAPbX_3$ crystals is stirred at 65 °C in presence of MAI, MABr or MACl (details reported in the SI).

Printed light detectors

We have used the formulated inks to print light signal detectors. We adopted a very simple planar architecture, where the $MAPbI_3$ crystals ink in IPA is deposited in ambient atmosphere by bar coating, a large-area and roll-to-roll compatible coating technique,[29, 37] on top of pre-patterned, interdigitated gold electrodes (Fig. 3a, Fig. S2). Such devices have almost symmetric current-voltage (*I-V*) characteristics and show light sensitivity when exposed to a monochromatic radiation at 532 nm of 1 mW/cm^2 (Fig. 3c). The spectral responsivity $R(\lambda)$ is comprised between 0.1 and 1 A/W (Fig. 3d) from 400 nm to 800 nm (applied bias of 5 V). These performances are drastically improved when we introduce a coating of the printed perovskite layer with the electron acceptor PCBM on top of the perovskite particles. Owing to the voids among particles, the solution permeates the few microns thick photoactive film, leading to a coverage of the surface of the printed perovskites particles with PCBM (Fig. 3b). As an effect, the photoresponse is drastically increased: the perovskite/PCBM detector shows a dark current of 9 nA, an order of magnitude higher than for the pristine perovskite (*vide infra*), and when the device is exposed to the same impinging radiation as before, the photocurrent

reaches 4.1 µA, three orders of magnitude more than in dark (Fig. 3c). As an example, PCBM deposited on top of a compact $MAPbI_3$ film produces only a marginal improvement owing to a much less extended perovskite/PCBM interface (Fig. S3). Such strong photoactivity of our printed $MAPbI_3$ crystals with the PCBM coating corresponds to a responsivity that varies between 10 A/W and 78.7 A/W within the spectral range from 400 nm to 820 nm, the latter corresponding to the absorption onset of the semiconductor (Fig. 3d). Such performances are reproducible over different printed photodetectors (Fig. S4). Moreover, the printed perovskite

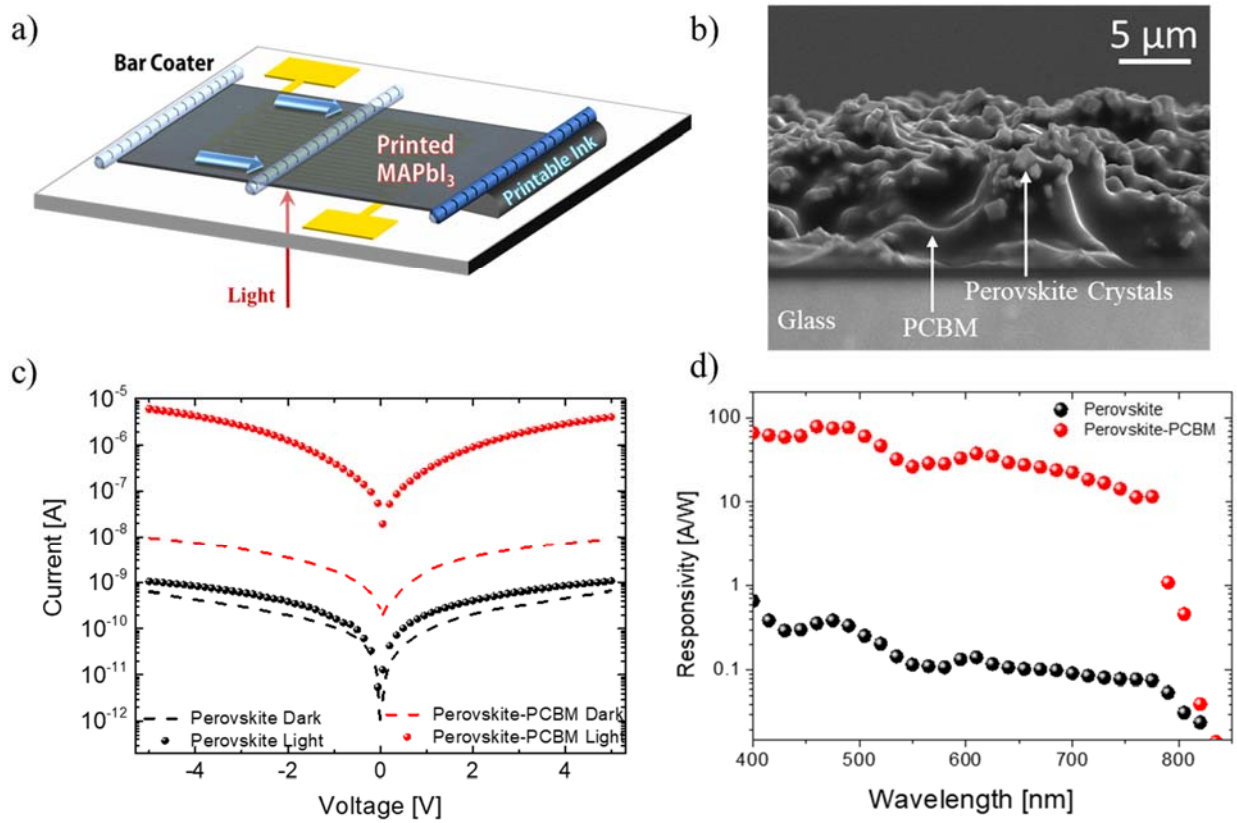

Fig. 3| *I-V*s and Responsivity of printed $MAPbI_3$ detectors. a, Schematic image of the perovskite photoconductor printed on a simple planar geometry with Au electrodes (channel width, W = 20 mm and channel length, L = 2.5 µm). **b**, Cross-sectional SEM image of the printed perovskite active layer with PCBM penetrating the crystals. **c**, Dark and light (532 nm LED light, 1mW/cm^2) *I-V* characteristic curves of the photoconductors with and without PCBM. **d**, Responsivity of the printed perovskite photodetectors with and without PCBM passivation at 5 V applied bias.

195 films stored in ambient conditions at a temperature of 300 K and at a relative humidity of 70
196 % does not show any measurable XRD peak of PbI_2 formation and show signature of hydration
197 only after 4 weeks (Fig. S5). Photodetectors show good stability under continuous illumination
198 for an observation time up to 1 h (Fig. S6).

199 Such high responsivity, achieved for a low applied bias voltage of 5 V over a channel length of
200 2.5 μm, suggests a gain mechanism.[38, 39] In fact, the external quantum efficiency (EQE)
201 calculated in the blue region of the spectrum exceeds 100 %. Such EQE value, together with
202 the symmetric *I* - *V* curves, indicates a photoconductive nature of the light detector. The external
203 gain (G_{ext}), defined as the unitless ratio between the number of collected photocarriers and the
204 number of incident photons,[38, 39] is estimated to be 213 at a wavelength (λ) equal to 460 nm
205 (Fig. S7). Such gain is one order of magnitude higher than in any printed perovskite
206 photodetector reported so far (Table 1). The photocurrent and G_{ext} as a function of the incident
207 light intensity are reported in Fig. 4a. At the low excitation density of 2 μW/cm^2 (λ = 560 nm),
208 the gain increases from about 6, in the case of the pristine perovskite device, to 180, when the
209 perovskite is coated with PCBM. With the light intensity increasing of almost 6 orders of
210 magnitude, the gain quickly vanishes below 1 for the pristine material, while such decrease is
211 strongly limited in presence of PCBM, with a gain which is still higher than 1 above 1 W/cm^2
212 (G_{ext} = 1.44 at 1.31 W/cm^2). Moreover, with addition of PCBM, the photocurrent is a power
213 law of light intensity, i.e. $\propto I^{\alpha}$ with $\alpha \approx 0.7$, on the base of which it is possible to retrieve the
214 input light signal from the recorded photocurrent.[40, 41, 42]

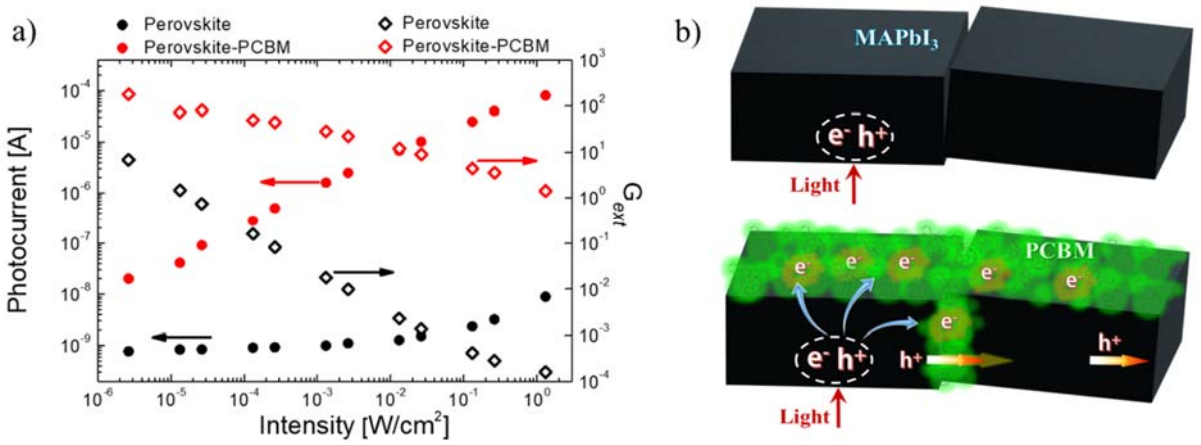

215

216 **Fig. 4| Intensity Dependent Gain. a**, Photocurrent and G_{ext} as a function of a constant incident
217 laser light intensity at λ = 560 nm for photoconductors with and without PCBM. **b**, Schematic
218 representation of the photoconduction mechanism: PCBM serves a dual role of acting as an
219 acceptor and trap for photogenerated electrons, and as passivation of particles surface traps,
220 thus facilitating holes transport and boosting both G_{ext} and Bandwidth of the detectors.

221

222 In a photoconductor the gain originates from a strong unbalance in the transport properties of
223 the photogenerated holes and electrons following the absorption of a photon, where one of the
224 two carriers is deeply trapped, and the other can drift under the external field.[38, 39] Once the
225 mobile carrier is collected at the electrode, another carrier is injected for charge neutrality.
226 Recirculation of the mobile carrier proceeds until the trapped carrier is finally released,
227 determining the gain that is proportional to the ratio between the de-trapping time and the
228 transit time. The presence of unbalanced charge transport in pristine $MAPbI_3$ upon photo-
229 excitation has been recently reported;[43, 44] moreover, the high work function of Au used for the
230 electrodes introduces a high energy barrier for injection of electrons for photoconduction, while
231 favoring recirculation of holes. This explains the behavior observed for the detector based on
232 pristine perovskite. At low light intensity the gain is high since trapping of one of the two
233 carriers by defect states and selective barrier for electrons at the contact unbalance the transport.

As traps are filled with increasing intensity, the transport becomes more balanced and/or the trapping time of the less mobile carrier reduces and the gain is correspondingly smaller. As largely reported in literature,[45, 46] PCBM has a passivation effect when deposited on the perovskite thin film (Fig. 4b). In fact, as a Lewis acid it is able to oxidize negatively charged PbI_3^- antisites or under-coordinated halide ions which work as deep traps for holes.[47] Therefore, by penetrating through the porous film of perovskite particles (Fig. 3b), it significantly improves the hole conductivity allowing the carriers to more easily drift through the particles under the externally applied bias: this explains the 10-fold increase in dark current. Simultaneously, it also acts as a sink by extracting photogenerated electrons from the perovskites phase. In such a way, the lifetime of the free holes in the perovskite is further increased, while electrons are confined in the PCBM phase with short diffusion length. All this results in a 30 times enhancement in gain at low excitation density (~ $\mu W/cm^2$), and in a G_{ext} still higher than 1 at high excitation density (~ W/cm^2). Since electrons are extracted from the perovskites phase in the PCBM treated device, the device is less sensitive to light intensity, explaining the markedly different intensity dependence of photocurrent and gain between pristine and PCBM coated perovskite.

As photoconductors are characterized by a trade-off between gain and response speed, or bandwidth, it is important to assess the transient time response of our printed perovskite/PCBM detectors. We evaluated the time response by irradiating the samples with a light pulse train with 500 µs pulse width and recording the transient photoresponse. The printed detectors follow very well the train of pulses (Fig. 5a, Fig. S8). The rise and fall times of the photoconductor with PCBM, defined as the time taken by the photocurrent to rise from 10 % to 90 % of the regime value, and vice-versa, are 14 µs in both cases (Fig. 5b). This photo-response is more than one order of magnitude faster than in previously reported printed perovskite photodetectors (Table 1). Such response time would allow the detector to follow

light signals with frequencies up to $f_{max} \approx 35$ kHz. Notably, despite the higher gain, it is about 4 time faster with respect to a device which uses only pristine perovskite (rise time about 55 µs, $f_{max} \approx 9$ kHz, Fig. S8). A decrease in transient response time with PCBM, and a concomitant increase of the gain, corroborate our picture of an improvement of the transport mechanism for holes within the perovskite layer, and an effective trapping of electrons in the acceptor PCBM phase. We have calculated the Gain–Bandwidth product of our detector, a figure of merit useful to compare combined performances of detectors with gain.[34] We obtain values as high as 7×10^6 Hz at 10 µW/cm^2 for λ = 460 nm, which is a few orders of magnitude higher than previously reported printed perovskite photodetectors. With respect to all perovskite photodetectors reported so far, irrespectively of the fabrication process, our device photodetector shows one of the most optimized Gain-Bandwidth tradeoff (Fig. S9).

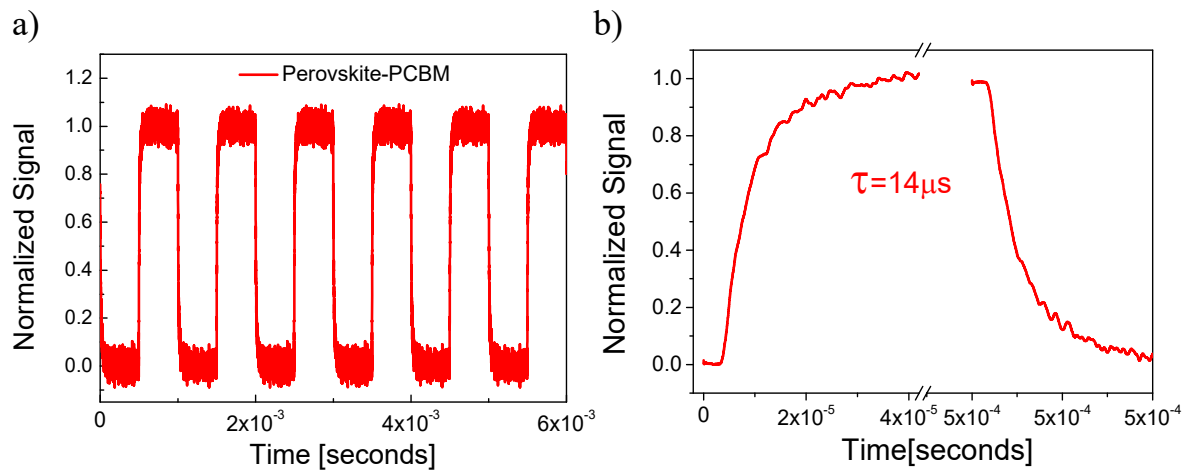

Fig. 5| Detector Transient Response. a, Response of the perovskite-PCBM detector to a light pulse train (532 nm LED, 500 µs pulse width, 1 µW/cm^2 intensity) with 5 V bias. **b**, Transient response of the photodetector with equal rise and fall times of 14 µs.

Noise characterization and Specific Detectivity

Another key feature of a light detector is related to its sensitivity, namely the possibility of detecting small signals. The minimum signal for which an electrical response is discernable is ultimately limited by the intrinsic device noise. One of the most adopted figure of merits to quantify this aspect is the Specific Detectivity (D^*), which normalizes the Noise Equivalent Power (NEP), *i.e.* the power of a sinusoidal monochromatic radiation producing the same r.m.s. output signal of the device current noise (i_n) in an ideal noise-less device over a Δf bandwidth, to the active area (A):

$$NEP = \frac{(\overline{i_n^2})^{0.5}}{R(\Delta f^{0.5})} [\mathrm{W}]/[Hz^{0.5}]$$

$$D^* = \frac{(A)^{0.5}}{NEP} \ [\mathrm{cmHz^{0.5}}]/[\mathrm{W}]$$

First estimations of D^* can be obtained by assuming that the limiting noise is represented by the white shot noise owing to fluctuations of the dark current. However, this approximation may lead to large overestimation of D^*,[8] especially at low frequencies where $1/f$ noise, so called "flicker" noise can be significant. Such scenario is even more critical for photoconductors, since traps, at the base of photoconduction, can significantly contribute to the flicker noise,[6, 9] pushing the corner frequency (f_c) between $1/f$ and the white shot noise, *i.e.* the frequency above which shot noise dominates D^*, to high frequency. If the device cannot operate at such high frequency, the assumption that white noise dominates completely fails. Therefore, D^* has to be quantitatively evaluated by performing accurate noise measurements. We have measured the equivalent current noise of both printed perovskite detectors, with and without PCBM, over a large bandwidth (10 Hz - 150 kHz, details on the measurements are reported in the Supplementary Information), with the aim to assess the effect of the organic coating on noise as well. In the investigated range, the noise of the printed detector without PCBM is completely dominated by flicker noise, thus reaching high level of noise over the whole bandwidth at which the detector can be operated (Fig. 6a). At the maximum operative frequency of 9 kHz for the

pristine perovskite device $(\overline{\imath_n^2})^{0.5}$ is ~ 1.1 x 10^{-13} A, almost two orders of magnitude higher than the shot noise, corresponding to a NEP of 0.16 pW/Hz$^{0.5}$, by assuming a 1 Hz bandwidth. Very interestingly, when the PCBM coating is introduced, the flicker noise is reduced by almost two orders of magnitude, so that f_c is retroceded within the investigated range, falling at 4 kHz (Fig. 6a). Since the perovskite-PCBM device can be operated up to 35 kHz, there is a frequency window from f_c up to such maximum frequency where the noise in the device is

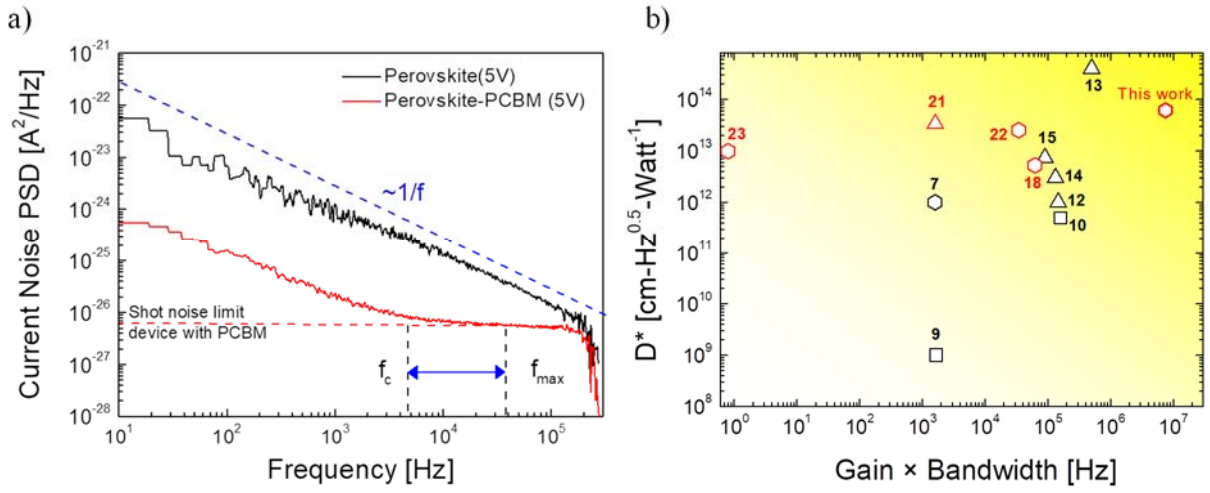

Fig. 6| Noise characteristics and device performance comparison. a, Current Noise Power Spectral Density (PSD) of the photoconductors with and without PCBM. Shot noise limit, corner frequency f_c, maximum operating frequency f_{max}, and frequency range where detectors are operated at shot noise limit is shown for devices with PCBM. **b,** Comparison chart for all types of perovskite photodetectors including the best performing printed photodetectors from all technologies including perovskites. Only devices with measured D^* are included. Red symbols: Best Printed Detectors; Black symbols: Non-Printed perovskite detectors; ⬡: Metal-Semiconductor-Metal Photoconductors; □: Photo-Gated Transistors; Δ: Photodiodes. References numbers correspond to the list reported in the Supporting Information, where a complete comparative table and method for comparison is reported.

limited purely by the shot noise. This results into a considerably lower $(\overline{\imath_n^2})^{0.5}$ of ~ 7.5 x 10^{-14} A above f_c, with a NEP of 0.95 fW/Hz$^{0.5}$, despite of the higher dark current observed in devices with PCBM (Fig. 3c). Considerable reduction of 1/f noise upon interfacing perovskite crystals with PCBM is an interesting evidence and confirms that PCBM acts as a trap passivation (Fig. 4b).[45, 46] We can suggest that PCBM acts on surface trap states of the crystals, which determines the higher flicker noise in the device without PCBM.[48] We compared the device noise, where the flicker noise dominates (500 Hz), with the noise expected from the Hooge's empirical formula, used to rationalize the 1/f noise in terms of fluctuations in the electrical conductance of homogeneous samples: $\left(\overline{\imath_n^2}\right) = \alpha_H I^\gamma/(fN)$ (Fig. S10),[49] where α_H is Hooge's parameter, I is the dark current, N is the total number of carriers. In the case of the pristine perovskite device, the Hooge's formula hardly fits the data, and $\gamma > 2$ is extracted on a limited range of currents and frequencies (Fig. S10). A value of γ exceeding 2 is seldom observed in literature, and may suggest a complex source of noise.[48, 49, 50] When PCBM is introduced, the low frequency flicker noise correlates well with the Hooge's formula for homogeneous samples (γ = 2, Fig. S10). Accumulation of ions at the grain boundaries in the presence of electric field have been consistently observed in $MAPbI_3$ thin films.[51] This effect would be exacerbated in the case of the pristine perovskite film, where the connectivity between individual perovskite crystals is lower than in spin coated films. Large presence of accumulated I^- ions at the grain boundaries is expected to give rise to inhomogeneity in energy landscapes, contributing to an increased noise. The passivation of ions by the presence of PCBM strongly reduces this source of noise, and renders γ equal to 2, as often verified in inorganic elemental semiconductors.

Thanks to the noise measurement, we can extract the specific detectivity D^*, which for the perovskite-PCBM detector is very high in all visible spectrum, reaching a maximum of 7.23 x 10^{13} cmHz$^{0.5}$/W at λ = 460 nm (Fig. S11). Our printed perovskite particles device shows one of the highest measured D^* for all perovskites detectors reported till date (Table S1) and is at

least one order of magnitude higher than any printed perovskite photodetector (Table 1). In Fig. 6b (Table S1) we plot D^* versus the Gain-Bandwidth product, in our case and for the best perovskite photodetectors reported so far where such figures of merit have been reported. We also compare the performance with state of the art printed photodetectors from established technologies such as quantum dots/nanocrystals and organic photodetectors with highest measured *D**. The very good overall performance of our detector is a consequence of a unique combination of trap passivation by PCBM, that reduces both the mobile (holes) carrier transit time and the 1/*f* noise, while simultaneously acting as an electron acceptor ensuring a selective hole circulation to achieve high gain.

Table 1: Main figure of merits of printed perovskite photodetectors with the highest *D** reported in literature and in this work. Theoretical calculated *D** by assuming shot noise limitation are marked with "!".

Printing Technique	*R* (A/W)	G_{ext}	Resp. time (µs)/ Bandwidth (Hz)	Detectivity × 10^{10} cm$Hz^{0.5}$/W	Intensity [/cm^2]	Voltage Applied	Ref. #
Roll-to-Roll Gravure	5.2×10^{-3}	-	-	-	36,000 µW	10 V	14
Inkjet Printing	1.2	2.3	10,000 µs	239(!)	100 µW	10 V	15
Blade Coating	13.5	30	240 µs	524	500 µW	5 V	16
Blade Coating and Hot Casting	8.95	20.9	7700 µs	290(!)	3700 µW	10 V	17
Blade Coating	10.75	25	9000 µs	-	-	10 V	18
Bar-coating	78.7	213	14 µs	7230	10 µW	5 V	This Work

Conclusions

In summary, we have formulated inks based on sub-micrometer organic-inorganic perovskite particles first synthetized in water and isopropanol and then dispersed in non-hazardous alcohol solvents. Simple planar light detectors were fabricated by printing the perovskite active phase by means of bar-coating, a large area and roll-to-roll compatible technique. The obtained devices show excellent photoconducting response when the active phase is functionalized with PCBM. The fullerene derivative on the one hand passivate hole traps, enhancing hole transport and reducing the rise and fall time to 14 μs, corresponding to a maximum operation frequency of 35 kHz; on the other, it acts as an acceptor phase for electrons, thus increasing the photoconductive gain. As a result, the device achieves a record high gain-bandwidth product of 7.5×10^6 Hz for printed perovskite light detectors. Importantly, the defects passivation also strongly suppresses 1/*f* noise, so that shot noise dominates already above 4 kHz. Thanks to the good dynamic response, the device can be operated in such frequency region, reaching the very high specific detectivity of 7.23 x 10^{13} cmHz$^{0.5}$/W which is the highest measured *D** for any printed photodetector till date.

Thanks to our perovskite particles inks we therefore demonstrate the fastest printed perovskite detector and the highest gain-bandwidth product so far. Moreover, the specific detectivity values observed are higher than commercially available silicon photodiodes, which is remarkable considering our photoconductor is printed with a very simple geometry. Our work therefore opens up attractive possibilities to use printable perovskites for large area light detection applications.

Acknowledgements

V.V., P.T. and A.P. would like to acknowledge funding from the DESTINY network within the European Union Seventh Framework Programme [FP7/2007-2013] under grant agreement

316494. Authors are thankful to Michele De Bastiani, Marina Gandini and Nikhil Tiwale for useful discussions.

Authors Contributions

P.T. and R.S. synthesized and characterized the materials, produced and printed the inks on inter-digitated electrodes prepared by D.N.. V.V. developed the fullerene passivation, performed all photodetector measurements and analyzed photodetector results with M.C. and A.P. . V.V. performed noise measurements and analyzed the data with G.F. and M.C. . V.V. and S.N. performed intensity dependent measurements. M.C. and A.P. guided the project. All the authors contributed to draft and revised the manuscript.

References:

1. Kim, H.-S., et al. Lead Iodide Perovskite Sensitized All-Solid-State Submicron Thin Film Mesoscopic Solar Cell with Efficiency Exceeding 9%. *Sci. Rep.* **2**, 591 (2012).

2. Lee, M. M., et al. Efficient Hybrid Solar Cells Based on Meso-Superstructured Organometal Halide Perovskites. *Science* **338**, 643-647 (2012).

3. NREL Efficiency Chart-https://www.nrel.gov/pv/assets/images/efficiency-chart.png. (2018).

4. Zhu, H., et al. Lead halide perovskite nanowire lasers with low lasing thresholds and high quality factors. *Nature Materials* **14**, 636 (2015).

5. Dou, L., et al. Solution-processed hybrid perovskite photodetectors with high detectivity. *Nature Communications* **5**, 5404 (2014).

6. Saidaminov, M. I., et al. Planar-integrated single-crystalline perovskite photodetectors. *Nature Communications* **6**, 8724 (2015).

7. Fang, Y., Huang, J. Resolving Weak Light of Sub-picowatt per Square Centimeter by Hybrid Perovskite Photodetectors Enabled by Noise Reduction. *Advanced Materials* **27**, 2804-2810 (2015).

8. Sutherland, B. R., et al. Sensitive, Fast, and Stable Perovskite Photodetectors Exploiting Interface Engineering. *ACS Photonics* **2**, 1117-1123 (2015).

9. Lin, Q., et al. Low Noise, IR-Blind Organohalide Perovskite Photodiodes for Visible Light Detection and Imaging. *Advanced Materials* **27**, 2060-2064 (2015).

10. Wang, H., Kim, D. H. Perovskite-based photodetectors: materials and devices. *Chemical Society Reviews* **46**, 5204-5236 (2017).

11. Chen, P.-Y., et al. Environmentally responsible fabrication of efficient perovskite solar cells from recycled car batteries. *Energy & Environmental Science* **7**, 3659-3665 (2014).

12. Binek, A., et al. Recycling Perovskite Solar Cells To Avoid Lead Waste. *ACS Applied Materials & Interfaces* **8**, 12881-12886 (2016).

13. Gardner Kira, L., et al. Nonhazardous Solvent Systems for Processing Perovskite Photovoltaics. *Advanced Energy Materials* **6**, 1600386 (2016).

14. Hu, Q., et al. Large-area perovskite nanowire arrays fabricated by large-scale roll-to-roll micro-gravure printing and doctor blading. *Nanoscale* **8**, 5350-5357 (2016).

15. Liu, Y., et al. Inkjet-Printed Photodetector Arrays Based on Hybrid Perovskite CH3NH3PbI3 Microwires. *ACS Applied Materials & Interfaces* **9**, 11662-11668 (2017).

16. Deng, W., et al. Aligned Single-Crystalline Perovskite Microwire Arrays for High-Performance Flexible Image Sensors with Long-Term Stability. *Advanced Materials* **28**, 2201-2208 (2016).

17. Tong, S., et al. Large-area and high-performance CH3NH3PbI3 perovskite photodetectors fabricated via doctor blading in ambient condition. *Organic Electronics* **49**, 347-354 (2017).

18. Li, S., et al. Fast-response and high-responsivity FAxMA(1−x)PbI3 photodetectors fabricated via doctor-blading deposition in ambient condition. *Organic Electronics* **52**, 190-194 (2018).

19. Akkerman, Q. A., et al. Strongly emissive perovskite nanocrystal inks for high-voltage solar cells. *Nature Energy* **2**, 16194 (2016).

20. Jang, D. M., et al. Reversible Halide Exchange Reaction of Organometal Trihalide Perovskite Colloidal Nanocrystals for Full-Range Band Gap Tuning. *Nano Letters* **15**, 5191-5199 (2015).

21. Minh, D. N., et al. Room-Temperature Synthesis of Widely Tunable Formamidinium Lead Halide Perovskite Nanocrystals. *Chemistry of Materials* **29**, 5713-5719 (2017).

22. Lamberti, F., et al. High-Quality, Ligands-Free, Mixed-Halide Perovskite Nanocrystals Inks for Optoelectronic Applications. *Advanced Energy Materials* **7**, 1601703 (2016).

23. Prochowicz, D., et al. Mechanosynthesis of the hybrid perovskite CH3NH3PbI3: characterization and the corresponding solar cell efficiency. *Journal of Materials Chemistry A* **3**, 20772-20777 (2015).

24. Bhooshan Kumar, V., et al. Sonochemical synthesis of CH3NH3PbI3 perovskite ultrafine nanocrystal sensitizers for solar energy applications. *Ultrasonics Sonochemistry* **32**, 54-59 (2016).

25. Kesari, Y., Athawale, A. Ultrasound assisted bulk synthesis of CH3NH3PbI3 perovskite at room temperature. *Materials Letters* **159**, 87-89 (2015).

26. Jang, D. M., et al. Ultrasound synthesis of lead halide perovskite nanocrystals. *Journal of Materials Chemistry C* **4**, 10625-10629 (2016).

27. Hintermayr Verena, A., et al. Tuning the Optical Properties of Perovskite Nanoplatelets through Composition and Thickness by Ligand-Assisted Exfoliation. *Advanced Materials* **28**, 9478-9485 (2016).

28. Davis, G. A., L. Kincaid, et al. Chemical Hazard Evaluation for Management Strategies: A Method for Ranking and Scoring Chemicals by Potential Human Health and Environmental Impacts. *Office of Research and Development, Cincinnati, OH* **EPA/600/R-94/177**, (1994).

29. Khim, D., et al. Simple Bar-Coating Process for Large-Area, High-Performance Organic Field-Effect Transistors and Ambipolar Complementary Integrated Circuits. *Advanced Materials* **25**, 4302-4308 (2013).

30. Pierre, A., et al. High Detectivity All-Printed Organic Photodiodes. *Advanced Materials* **27**, 6411-6417 (2015).

31. Konstantatos, G., et al. Ultrasensitive solution-cast quantum dot photodetectors. *Nature* **442**, 180 (2006).

32. Zhang, Q., et al. Solution-Processed Graphene Quantum Dot Deep-UV Photodetectors. *ACS Nano* **9**, 1561-1570 (2015).

33. Giuseppina, P., et al. Printed photodetectors. *Semiconductor Science and Technology* **30**, 104006 (2015).

34. García de Arquer, F. P., et al. Solution-processed semiconductors for next-generation photodetectors. *Nature Reviews Materials* **2**, 16100 (2017).

35. Clusters in solution: Growth and optical properties of layered semiconductors with hexagonal and honeycombed structures. *The Journal of Chemical Physics* **85**, 5337-5340 (1986).

36. Ha, S. T., et al. Synthesis of Organic–Inorganic Lead Halide Perovskite Nanoplatelets: Towards High-Performance Perovskite Solar Cells and Optoelectronic Devices. *Advanced Optical Materials* **2**, 838-844 (2014).

37. Bucella, S. G., et al. Macroscopic and high-throughput printing of aligned nanostructured polymer semiconductors for MHz large-area electronics. *Nat. Commun.* **6**, 8394 (2015).

38. Konstantatos, G., Sargent, E. H. Nanostructured materials for photon detection. *Nature Nanotechnology* **5**, 391 (2010).

39. Liu, J.-m. *Photonic Devices*. Cambridge University Press: Cambridge, 2005.

40. Jie, J. S., et al. Photoconductive Characteristics of Single-Crystal CdS Nanoribbons. *Nano Letters* **6**, 1887-1892 (2006).

41. Irkhin, P., Najafov, H., Podzorov, V. Steady-state photoconductivity and multi-particle interactions in high-mobility organic semiconductors. *Scientific Reports* **5**, 15323 (2015).

42. Stöckmann, F. On the Dependence of Photocurrents on the Excitation Strength. *physica status solidi (b)* **34**, 741-749 (1969).

43. Leijtens, T., et al. Carrier trapping and recombination: the role of defect physics in enhancing the open circuit voltage of metal halide perovskite solar cells. *Energy & Environmental Science* **9**, 3472-3481 (2016).

44. Meggiolaro, D., et al. Iodine chemistry determines the defect tolerance of lead-halide perovskites. *Energy & Environmental Science* **11**, 702-713 (2018).

45. Zheng, X., et al. Defect passivation in hybrid perovskite solar cells using quaternary ammonium halide anions and cations. *Nature Energy* **2**, 17102 (2017).

46. De Bastiani, M., et al. Ion Migration and the Role of Preconditioning Cycles in the Stabilization of the J–V Characteristics of Inverted Hybrid Perovskite Solar Cells. *Advanced Energy Materials* **6**, 1501453 (2015).

47. Du, M.-H. Density Functional Calculations of Native Defects in CH3NH3PbI3: Effects of Spin–Orbit Coupling and Self-Interaction Error. *The Journal of Physical Chemistry Letters* **6**, 1461-1466 (2015).

48. Hooge, F. N., Kleinpenning, T. G. M., Vandamme, L. K. J. Experimental studies on 1/f noise. *Reports on Progress in Physics* **44**, 479 (1981).

49. Ziel, A. v. d. Unified presentation of 1/f noise in electron devices: fundamental 1/f noise sources. *Proceedings of the IEEE* **76**, 233-258 (1988).

50. Liu, G., et al. Origin of 1/f noise in graphene multilayers: Surface vs. volume. *Applied Physics Letters* **102**, 093111 (2013).

51. Yuan, Y., Huang, J. Ion Migration in Organometal Trihalide Perovskite and Its Impact on Photovoltaic Efficiency and Stability. *Accounts of Chemical Research* **49**, 286-293 (2016).